Neurobiology of Aging 75 (2019) 187–197

Contents lists available at ScienceDirect

Neurobiology of Aging

journal homepage: www.elsevier.com/locate/neuaging

^{18}F-flortaucipir uptake patterns in clinical subtypes of primary progressive aphasia

Hanna Cho [a], Hee Jin Kim [b], Jae Yong Choi [c,d], Young Hoon Ryu [c], Myung Sik Lee [a], Duk L. Na [b], Sang Won Seo [b,*], Chul Hyoung Lyoo [a,**]

[a] Department of Neurology, Gangnam Severance Hospital, Yonsei University College of Medicine, Seoul, Republic of Korea
[b] Departments of Neurology, Samsung Medical Center, Sungkyunkwan University School of Medicine, Seoul, Korea
[c] Department of Nuclear Medicine, Gangnam Severance Hospital, Yonsei University College of Medicine, Seoul, Republic of Korea
[d] Division of RI-Convergence Research, Korea Institute Radiological and Medical Sciences, Seoul, South Korea

ARTICLE INFO

Article history:
Received 6 February 2018
Received in revised form 14 November 2018
Accepted 15 November 2018
Available online 23 November 2018

Keywords:
Primary progressive aphasia
^{18}F-flortaucipir
Tau
Positron emission tomography

ABSTRACT

We analyzed ^{18}F-flortaucipir uptake patterns and structural changes in patients with subtypes of primary progressive aphasia (PPA) using ^{18}F-flortaucipir positron emission tomography and volumetric magnetic resonance imaging. We enrolled 34 consecutive patients with PPA (10 nonfluent/agrammatic PPA [nfvPPA], 18 semantic variant PPA [svPPA], and 6 logopenic variant PPA [lvPPA], as well as 20 healthy controls, and 20 patients with Alzheimer's disease. ^{18}F-flortaucipir uptake was increased in the frontal cortex and underlying white matter, and subcortical nuclei in the 10 nfvPPA and 8 nfvPPA-amyloid-β (Aβ)− subgroup patients. In the svPPA patients (both the 13 svPPA-Aβ− and 5 svPPA-Aβ+), uptake generally increased in the widespread neocortex with left anterior temporal predominance. ^{18}F-flortaucipir uptake patterns in the 6 lvPPA and the 5 lvPPA-Aβ+ subgroup patients were similar to those seen in the patients with Alzheimer's disease with mild predominance in the left lateral temporal cortex. Cortical thinning in each PPA subtype corresponded with increased ^{18}F-flortaucipir uptake. ^{18}F-flortaucipir uptake patterns and cortical atrophy were distinct and corresponded to areas related to the specific language functions that are impaired in each subtype of PPA.

1. Introduction

Primary progressive aphasia (PPA) is a clinical syndrome characterized by predominant language dysfunction but with other cognitive functions relatively preserved (Mesulam, 2001). PPA can be classified into 3 subtypes based on characteristics of language impairment, which include the nonfluent/agrammatic variant PPA (nfvPPA), semantic variant PPA (svPPA), and logopenic variant PPA (lvPPA) (Gorno-Tempini et al., 2004, 2011).

PPA clinical syndromes are linked to underlying frontotemporal lobar degeneration (FTLD) tau, TAR DNA-binding protein 43 (TDP43), and Alzheimer's disease (AD) pathology (Grossman, 2010). FTLD-tau pathology is predominantly observed in nfvPPA, whereas svPPA and lvPPA are highly suggestive of TDP43 and AD pathologies, respectively. Although postmortem studies have shown proportional variability of these pathologies in the different PPA subtypes, with the exception of svPPA, which has a smaller proportion of FTLD-tau (0%–17%) or AD (10%–33%) tau pathology, over 75% of patients with nfvPPA harbor FTLD-tau (50%–100%) or AD (13%–41%) tau pathology, and approximately 85% of patients with lvPPA exhibit FTLD-tau (0%–29%) or AD (54%–77%) tau or TDP43 (14%–27%) pathology (Chare et al., 2014; Harris et al., 2013; Josephs et al., 2006, 2014; Kertesz et al., 2005; Knibb et al., 2006; Mesulam et al., 2008; Rohrer et al., 2010, 2011).

The development of tau radiotracers has enabled in vivo visualization of tau pathology in various neurodegenerative diseases (Cho et al., 2017; Johnson et al., 2016; Passamonti et al., 2017; Smith et al., 2016). ^{18}F-flortaucipir (formerly called ^{18}F-AV-1451 or ^{18}F-T807) has been the most widely used tau radiotracer. It strongly binds to paired helical filament tau predominantly found in patients with AD and weakly binds to straight filament tau found in non-AD tauopathies (Marquie et al., 2015), while even weakly binding to TDP43 pathology (Lowe et al., 2016).

Recently, the possibility of binding to monoamine oxidase-B has been raised, which can colocalize with neurodegeneration (Bevan-Jones et al., 2017).

* Corresponding author at: Department of Neurology, Samsung Medical Center, Sungkyunkwan University School of Medicine, 81 Irwonro, Gangnam-gu, Seoul, South Korea. Tel.: +82-2-3410-1233; fax: +82-2-3410-0052.
** Corresponding author at: Department of Neurology, Gangnam Severance Hospital, Yonsei University College of Medicine, 20 Eonjuro 63-gil, Gangnam-gu, Seoul, South Korea. Tel.: +82-2-2019-3326; fax: +82-2-3462-5904.
E-mail addresses: sangwonseo@empas.com (S.W. Seo), lyoochel@yuhs.ac (C.H. Lyoo).

0197-4580/$ – see front matter © 2018 Elsevier Inc. All rights reserved.
https://doi.org/10.1016/j.neurobiolaging.2018.11.017

Therefore, ^{18}F-flortaucipir may be helpful for observing AD tau pathology, whereas the binding to FTLD-tau pathology in most patients with nfvPPA and the binding to TDP43 pathology in some patients with svPPA are difficult to accurately identify by ^{18}F-flortaucipir.

Although ^{18}F-flortaucipir binding patterns in small numbers of patients with lvPPA and svPPA have been reported in separate studies (Bevan-Jones et al., 2017; Makaretz et al., 2018; Nasrallah et al., 2018; Ossenkoppele et al., 2016; Xia et al., 2017), to date, only one study with ^{18}F-flortaucipir positron emission tomography (PET) has collectively analyzed binding patterns in different PPA subtypes (Josephs et al., 2018). However, the results may have been mixed due to AD pathology, and distinct ^{18}F-flortaucipir uptake patterns might still be determinable. In this study, we sought to investigate ^{18}F-flortaucipir uptake patterns and structural changes in PPA using volumetric and cortical thickness analysis. We also sought to investigate differences according to amyloid-positivity.

2. Methods

2.1. Participants

From May 2015 to Jan 2017, we prospectively recruited 34 consecutive patients with PPA at Gangnam Severance Hospital (7 patients) and at Samsung Medical Center (27 patients). By using the clinical diagnostic criteria for the diagnosis of PPA and its variants, patients with PPA were clinically diagnosed and classified into one of 3 variants (10 nfvPPA, 18 svPPA, and 6 lvPPA patients) (Gorno-Tempini et al., 2011). None of the patients had their clinical diagnosis changed during the follow-up period (mean follow-up period = 22.8 ± 7.0 months). All patients underwent detailed neuropsychological tests, genotyping for apolipoprotein E, magnetic resonance (MR) imaging, and 2 consecutive PET scans with ^{18}F-flortaucipir for tau and ^{18}F-florbetaben for amyloid-β (Aβ) on separate days. PET scans were performed for 20 minutes duration, beginning at 80 minutes after the injection of 285.6 ± 33.8 MBq of ^{18}F-flortaucipir and 90 minutes after the injection of 301.4 ± 35.5 MBq of ^{18}F-florbetaben. Aβ positivity was determined by agreement between 2 nuclear medicine specialists using a validated visual assessment method (Villemagne et al., 2011).

For comparison, we also included 20 Aβ-positive patients with AD and 20 Aβ-negative healthy controls after matching for age (±3) and performed the same clinical assessments and imaging studies. Patients with AD met the criteria for probable AD dementia with evidence of the AD pathophysiological process based on clinical assessments and Aβ positivity shown in ^{18}F-florbetaben PET images (McKhann et al., 2011). All patients with AD had amnestic AD and did not show any atypical clinical presentations such as logopenic aphasia, posterior cortical atrophy, or frontal variant AD. Healthy controls met Christensen's criteria, and none had a history of neurological or psychiatric illness, or abnormalities in MR images (Christensen et al., 1991). All controls showed normal performance in neuropsychological tests and were Aβ negative on ^{18}F-florbetaben PET. We used the same neuropsychological tests, protocols for the acquisition of PET and MR images, and image processing steps as in our previous work (Cho et al., 2016). Details of these methods are described in Supplemental Methods.

2.2. Standard protocol approvals, registrations, and patient consent

This study was approved by the Institutional Review Board of Gangnam Severance Hospital and Samsung Medical Center, and written informed consent was obtained from all participants.

2.3. Acquisition of PET and MR images

All ^{18}F-flortaucipir and 69 of 74 ^{18}F-florbetaben PET scans were performed with a Biograph mCT PET/computed tomography (CT) scanner (Siemens Medical Solutions; Malvern, PA, USA) at Gangnam Severance Hospital. Five patients with PPA underwent ^{18}F-florbetaben PET scans in a Discovery STE PET/CT scanner (GE Healthcare; Waukesha, WI, USA) at Samsung Medical Center. Before the PET scan, a head holder was applied to minimize head motion during the scan and CT images were acquired for later attenuation correction. After the corrections for attenuation, scatter and decay, the PET images acquired in the Biograph mCT scanner were reconstructed in a 256 × 256 × 223 matrix with 1.591 × 1.591 × 1 mm voxel size by using the ordered-subsets expectation maximization algorithm, and those acquired in the Discovery STE scanner were reconstructed in a 128 × 128 × 47 matrix with 2 × 2 × 3.27 mm voxel size by using the 3D-iterative reconstruction algorithm.

In a 3.0 Tesla MR scanner (Discovery MR750, GE Medical Systems, Milwaukee, WI, USA), T1-weighted MR images were acquired with 3D-spoiled gradient-recalled sequences (repetition time = 8.28 ms, echo time = 1.6–11.0 ms, flip angle = 20°, 512 × 512 matrix, voxel spacing 0.43 × 0.43 × 1 mm).

2.4. Image processing steps

FreeSurfer 5.3 (Massachusetts General Hospital, Harvard Medical School; http://surfer.nmr.mgh.harvard.edu) was used for processing of MR images. MR images were resliced to 1 mm isovoxel space in 256 × 256 × 256 matrix. Inhomogeneity-corrected and skull-stripped MR images were segmented into gray and white matters based on the intensity gradient and connectivity of voxels. Three-dimensional surfaces for cortical gray and white matters were modeled after tessellation with trigons, and then cortical thickness was mapped on white matter surface by measuring the distance between a vertex on white matter and its corresponding vertex on gray matter surface. Cortical gray matter was parcellated with probabilistic labeling algorithm based on curvature information (Desikan et al., 2006; Fischl et al., 2004), and subcortical structures were segmented with probabilistic registration technique (Fischl et al., 2002). By using these cortical and subcortical segments, volume-of-interest (VOI) masks for 112 cortical and subcortical structures were created. Finally, after merging the anatomically related regions, a participant-specific composite VOI mask for 19 cortical (superior, middle and inferior frontal, orbitofrontal, sensorimotor, superior and inferior parietal, precuneus, occipital, superior, middle and inferior temporal, anterior and posterior cingulate, entorhinal, parahippocampal cortices, amygdala, and hippocampus), and 5 subcortical regions (thalamus, caudate, putamen, globus pallidus, and cerebellar cortex). Regional volumes were measured by counting the voxels within each VOI, and cortical thickness was measured.

Statistical parametric mapping 8 (SPM8; Wellcome Trust Centre for Neuroimaging, London, UK) and in-house software implemented in MATLAB 7.1 (MathWorks, Natick, MA, USA) were used for processing the PET images. PET images were coregistered to the MR images. Standardized uptake value ratio (SUVR) images were created by dividing the voxel values by the mean binding value of the cerebellar cortex. Regional SUVR values were measured by overlaying the participant-specific composite VOI mask image on each SUVR image. We primarily analyzed regional SUVR values uncorrected for partial volume effect (PVE), but those corrected for PVE with the region-based voxelwise method were also analyzed (Thomas et al., 2011). By using the diffeomorphic anatomical registration using exponentiated lie algebra (DARTEL) toolbox in

SPM8, MR images were spatially normalized to in-house DARTEL template in 1 mm isovoxel space, and the SUVR images were also spatially normalized to the template space by applying the flow field, normalizing the gray and white matter segments extracted from MR images. Finally, normalized PET images were smoothed by Gaussian kernel with 8 mm full-width half maximum for the voxel-based comparison.

Cortical SUVR values were extracted from the voxels at the midpoint between the gray and white matter surfaces and mapped on the corresponding vertices of the white matter surface. Surface SUVR and cortical thickness maps were spatially normalized to the template surfaces and finally smoothed on 2D-surface by Gaussian kernel with 8 mm full-width half maximum for the surface-based analysis.

2.5. Statistical analysis

SPSS 23 (IBM Corp., Armonk, NY, USA) was used for statistical analysis. For groupwise comparison of demographic data, we used the Kruskal-Wallis test with Dunn's procedure for the comparison of continuous variables and chi-square test with Bonferroni's correction for the comparison of categorical variables.

We first compared regional SUVR values and volumes between the controls and 4 patient groups, and then after stratification by Aβ positivity, compared between the controls and 6 patient groups (nfvPPA-Aβ−, svPPA-Aβ−, svPPA-Aβ+, lvPPA-Aβ+, and AD). We did not include nfvPPA-Aβ+ or lvPPA-Aβ− groups for this comparison due to the very small number of patients within these 2 groups. For small numbers of patients in some of the PPA groups, we used rank-based non-parametric analysis of covariance statistics for the comparison between groups (Quade, 1967). To accomplish this, ranks were calculated for each dependent variable (regional SUVR values) and covariates (age and years of education). Unstandardized residuals for the ranks of each dependent variable were calculated using a linear regression model with ranks of 2 covariates as independent variables and then compared between groups with the multivariate general linear model. First, Bonferroni's method was used for groupwise correction for multiple comparisons, and then Benjamini-Hochberg's false discovery rate method was used for region-wise correction for multiple comparisons (Benjamini and Hochberg, 1995). In addition, regional asymmetry indices (AI) were calculated for ^{18}F-flortaucipir SUVR values and volumes as follows: AI (%) = (right−left)/(right + left) × 200. One sample *t*-test was used within groups. To investigate the correlation between test performance (naming and fluency) and regional ^{18}F-flortaucipir uptake, we calculated standardized residuals for each variable using a multivariate general linear model to adjust for age and education and used Pearson's correlation analysis between the standardized residuals derived from the language measurements and SUVR values.

Similarly, this nonparametric method was applied to voxel- and surface-based comparisons in the following order: (1) creation of rank maps, (2) creation of unstandardized residual maps, (3) group comparison using statistical tools in SPM8 (for voxel-based comparison) or FreeSurfer (for surface-based comparison), and (4) correction for multiple comparisons using the false discovery rate method.

3. Results

3.1. Demographic characteristics

Demographic characteristics and neuropsychological tests results of the 5 diagnostic groups are presented in Table 1. There was no difference across groups in terms of age, gender, education, or duration of disease. Apolipoprotein E ε4 genotype was more prevalent in the patients with AD than the controls. Global cognition scales and all neuropsychological test results were observed to differ between the groups ($p < 0.05$); however, after post hoc comparisons, there was no difference between the AD or other PPA groups, with the exception of the Boston Naming Test (BNT). The BNT result for the svPPA group was lower than that of the nfvPPA and AD groups. Amyloid-positivity was identified in 20% of the patients with nfvPPA, 28% of the patients with svPPA, and 83% of the patients with lvPPA. Detailed results of the PPA groups stratified by amyloid-positivity are presented in Table S1.

3.2. Comparison of cortical and subcortical ^{18}F-flortaucipir uptake

When compared to the controls, VOI-based analysis revealed characteristic ^{18}F-flortaucipir uptake patterns (Fig. 1). In the patients with nfvPPA, uptake was increased in the frontal, insula, and entorhinal cortices, and amygdala. Subcortical gray matter structures such as the thalamus, putamen, and globus pallidus also showed increased uptake. In the patients with nfvPPA-Aβ-, there was an increased uptake in the frontal cortices. The patients with svPPA showed increased uptake in the frontal, sensorimotor, precuneus, occipital, middle and inferior temporal, anterior and posterior cingulate, insula, entorhinal, parahippocampal cortices, amygdala, and putamen. Interestingly, after stratification by Aβ-positivity, the svPPA-Aβ− patients still showed increased uptake in the inferior frontal, orbitofrontal, middle and inferior temporal, entorhinal, parahippocampal, anterior and posterior cingulate, insula cortices and amygdala. The svPPA-Aβ+ patients showed highly increased uptake in all cortical regions except for the hippocampus with inferior temporal predominance. In the lvPPA and the subgroup lvPPA-Aβ+ patients, ^{18}F-flortaucipir uptake was increased in all cortical regions except for the hippocampus and the putamen with inferior temporal predominance. Patients with AD showed highly increased uptake in all cortical and subcortical regions except for the globus pallidus with medial temporal predominance. Effect size of regional ^{18}F-flortaucipir uptake values between the controls and each disease group was presented in Table S2. When we performed VOI analysis between the PPA groups on direct comparison, compared to the patients with nfvPPA, the patients with svPPA showed a trend toward increased uptake in the middle ($p = 0.027$) and inferior ($p = 0.025$) temporal cortices, whereas the patients with lvPPA showed a trend toward increased uptake in the occipital ($p = 0.042$), superior ($p = 0.015$), middle ($p = 0.015$), and inferior ($p = 0.004$) temporal cortices. Compared to the patients with svPPA, the patients with lvPPA showed only a trend toward increased uptake in the middle frontal ($p = 0.030$) cortex. However, none of the regions survived multiple comparisons (Table S3). The VOI analysis for each side is presented in Table S4. Statistical results were consistent even after adding gender as a covariate for the group comparison. The analysis of PVE-corrected data revealed almost identical results to those of the PVE-uncorrected data (Fig. S1).

Voxel- and surface-based comparisons also confirmed the increased ^{18}F-flortaucipir uptake patterns shown in the VOI-based analysis (Fig. 2). The nfvPPA and the subgroup nfvPPA-Aβ- patients showed increased uptake predominantly in the frontal subcortical white matter with mild right predominance and subcortical nuclei. However, in the patients with svPPA, the uptake was increased in the widespread frontotemporoparietal regions and ventral striatum with clear left anterior temporal predominance. Even in the svPPA-Aβ- patients, the uptake was also increased slightly in the lateral frontal cortex and highly in the anterior temporal cortex, predominantly in the left side. The svPPA-Aβ+ patients showed significantly increased uptake in the cortical

Table 1
Demographic characteristics of 5 diagnostic groups

Demographics	HC	nfvPPA	svPPA	lvPPA	AD
N	20	10	18	6	20
Age (y)	64.0 (57.5–69.8)	64.5 (56.3–79.0)	71.0 (63.0–74.5)	68.5 (58.0–79.0)	67.5 (63.0–69.0)
Gender (M:F)	8: 12	4: 6	10: 8	2: 4	4: 16
Right handedness (%)	20 (100%)	10 (100%)	18 (100%)	5 (80%)	20 (100%)
Education (y)	13.0 (12.0–16.0)	11.5 (5.3–14.5)	12.0 (6.8–15.3)	16.0 (4.5–16.5)	12.0 (6.8–16.0)
Duration (y)	n.a.	3.0 (2.0–3.3)	4.0 (2.8–7.0)	3.0 (2.5–4.0)	3.0 (3.0–4.0)
ApoE ε4 (%)	4/20 (20%)	1/9 (11%)	5/18 (28%)	1/6 (17%)	13/20 (65%)[a]
Amyloid positivity	0 (0%)	2 (20%)[b]	5 (28%)[b]	5 (83%)[a]	20 (100%)[a]
Global ^{18}F-flortaucipir SUVR	1.04 (1.01–1.06)	1.13 (1.06–1.20)	1.17 (1.07–1.69)[a]	1.67 (1.30–2.12)[a]	1.82 (1.38–2.00)[a]
Cognitive function tests (possible maximum score)					
MMSE	28.5 (28.0–30.0)	24.0 (7.0–28.0)[a]	15.5 (2.5–25.0)[a]	10.5 (0.0–14.8)[a]	17.5 (14.0–21.8)[a]
CDR-SB	0.5 (0.0–1.4)	2.8 (0.9–5.1)	4.8 (2.5–7.8)[a]	5.5 (4.1–8.8)[a]	5.3 (4.1–8.6)[a]
DS-BW (8)	4.0 (3.3–5.8)	3.0 (0.0–3.0)[a]	3.0 (2.0–3.0)[a]	2.0 (0.0–3.0)[c]	3.0 (2.0–3.0)[a]
BNT (60)	53.0 (52.0–57.0)	41.0 (27.5–49.3)	6.0 (1.0–11.0)[a,b]	5.5 (1.3–9.0)[a]	35.0 (28.0–44.0)[a]
RCFT (36)	34.5 (32.6–35.0)	15.0 (2.0–30.3)[a]	30.5 (26.5–34.0)	27.0 (3.0.- 27.5)[c]	10.5 (4.9–32.0)[a]
SVLT-DR (12)	7.5 (6.0–9.0)	1.5 (0.0–4.8)[a]	0.0 (0.0–0.0)[a]	0.5 (0.0–1.0)[a]	0.0 (0.0–0.0)[a]
RCFT-DR (36)	15.5 (11.6–21.8)	4.0 (0.5–17.1)	7.0 (0.0–10.5)[a]	1.0 (0.0–12.5)[c]	0.0 (0.0–1.5)[a]
COWAT	17.0 (14.0–19.0)	5.5 (2.0–10.5)[a]	4.0 (0.0–5.0)[a]	4.0 (0.8–5.8)[a]	9.0 (4.0–10.0)[a]

Continuous variables are presented with medians and interquartile ranges.
Key: AD, Alzheimer's disease; Aβ+/-, amyloid-positivity, ApoE, apolipoprotein E; BNT, Boston Naming Test; CDR-SB, Clinical Dementia Rating sum-of-boxes; COWAT, Controlled Oral Word Association Test-Semantics; DS-BW, Digit Span Backward; HC, healthy controls; lvPPA, logopenic variant PPA; MMSE, Mini-Mental State Examination; nfvPPA, nonfluent variant PPA; n.a., not applicable or not available; PPA, primary progressive aphasia; RCFT, Rey-Osterrieth Complex Figure Test; RCFT-DR, Rey-Osterrieth Complex Figure Test-Delayed Recall; SVLT-DR, Seoul Verbal Learning Test-Delayed Recall; svPPA, semantic variant PPA; SUVR, standardized uptake value ratio.
[a] $p < 0.05$ for the comparisons between the controls and each patient group.
[b] $p < 0.05$ for the comparisons between the AD and other PPA groups.
[c] Only a portion of the patients with lvPPA completed all of the cognitive function tests and the items presented with minimum and maximum values.

areas similar to the svPPA-Aβ− patients with predominance of the left anterior temporal cortex, and there was a trend for greater uptake in the left anterior temporal cortex even compared to AD. The lvPPA and the subgroup lvPPA-Aβ+ patients also showed moderately increased uptake in the widespread cortical regions with mild predominance in the left lateral temporal cortex. Patients with AD showed the most highly increased uptake in all cortical regions with predominance in the medial and inferior lateral temporal, inferior parietal, precuneus, and medial and lateral frontal cortices. In addition, ^{18}F-flortaucipir PET images of individual patients with PPA were presented in Fig. S3.

3.3. Comparison of cortical and subcortical volumes and cortical thickness

Surface-based cortical thickness analysis showed distinct patterns of cortical thinning in the subtypes of PPA groups (Fig. 3). Compared to the controls, cortical thinning was observed in the lateral frontal and medial temporal cortices in the nfvPPA and the subgroup nfvPPA-Aβ- with mild left-side predominance. Cortical thinning was most prominent in the patients with svPPA. Thicknesses of the inferior and lateral temporal and insula cortices were thinner than in the controls, and thinning in the anterior temporal cortex was most prominent. Interestingly, cortical thinning in the left anterior temporal cortex was greater in the svPPA-Aβ− patients than in the svPPA-Aβ+ patients and even greater than in the patients with AD. The svPPA-Aβ+ patients also showed cortical thinning in the left anterior temporal cortex to a lesser degree than in the svPPA-Aβ−, but thinning was extended to the inferior parietal cortex. Cortical thinning was much less prominent in the lvPPA and the subgroup lvPPA-Aβ+, and only slight thinning was observed in the inferior and medial temporal cortex and posterior cingulate cortices with a slight left predominance.

VOI-based regional volume analysis showed a less prominent regional volume loss pattern in PPA groups probably due to a dilution effect after averaging both sides of the hemisphere (Fig. S2). The nfvPPA and the subgroup nfvPPA-Aβ− patients showed mild volume atrophy only in the inferior frontal cortex compared to the controls, but this difference did not survive region-wise multiple comparisons. The svPPA and the subgroup svPPA-Aβ− patients commonly showed prominent volume atrophy in the lateral and medial temporal and insula cortices. However, the svPPA-Aβ+ patients showed mild atrophy in the inferior temporal, entorhinal, and parahippocampal cortices only before correcting for region-wise multiple comparisons. The patients with lvPPA showed mild atrophy in the inferior temporal, parahippocampal, and entorhinal cortices, but only the inferior temporal and parahippocampal cortices survived multiple comparisons. The lvPPA-Aβ+ patients showed a trend of volume atrophy in the inferior temporal and parahippocampal cortices, but the regions did not survive multiple comparisons.

3.4. Asymmetry of ^{18}F-flortaucipir uptake and cortical and subcortical volumes

Asymmetry of cortical ^{18}F-flortaucipir uptake and volume loss was assessed by AI (Fig. 4 and Table S6). In nfvPPA and nfvPPA-Aβ-, no significant asymmetry of cortical ^{18}F-flortaucipir uptake was observed, whereas the volumes of the left inferior parietal, precuneus, and middle temporal cortices were significantly smaller than those of the right side. Patients with svPPA and its subgroups showed left-side predominance for most cortical and subcortical ^{18}F-flortaucipir uptake and cortical volume atrophy, particularly in the inferior parietal, precuneus, and middle and inferior temporal cortices. Although the lvPPA patients did not reach statistical significance, when we analyzed AI in the lvPPA-Aβ+ subgroup patients (excluding one lvPPA-Aβ+ patient with right predominance), 4 lvPPA-Aβ+ patients showed significant asymmetry of left predominant ^{18}F-flortaucipir uptake in the superior and middle frontal, sensory-motor, and precuneus cortices (Table S6).

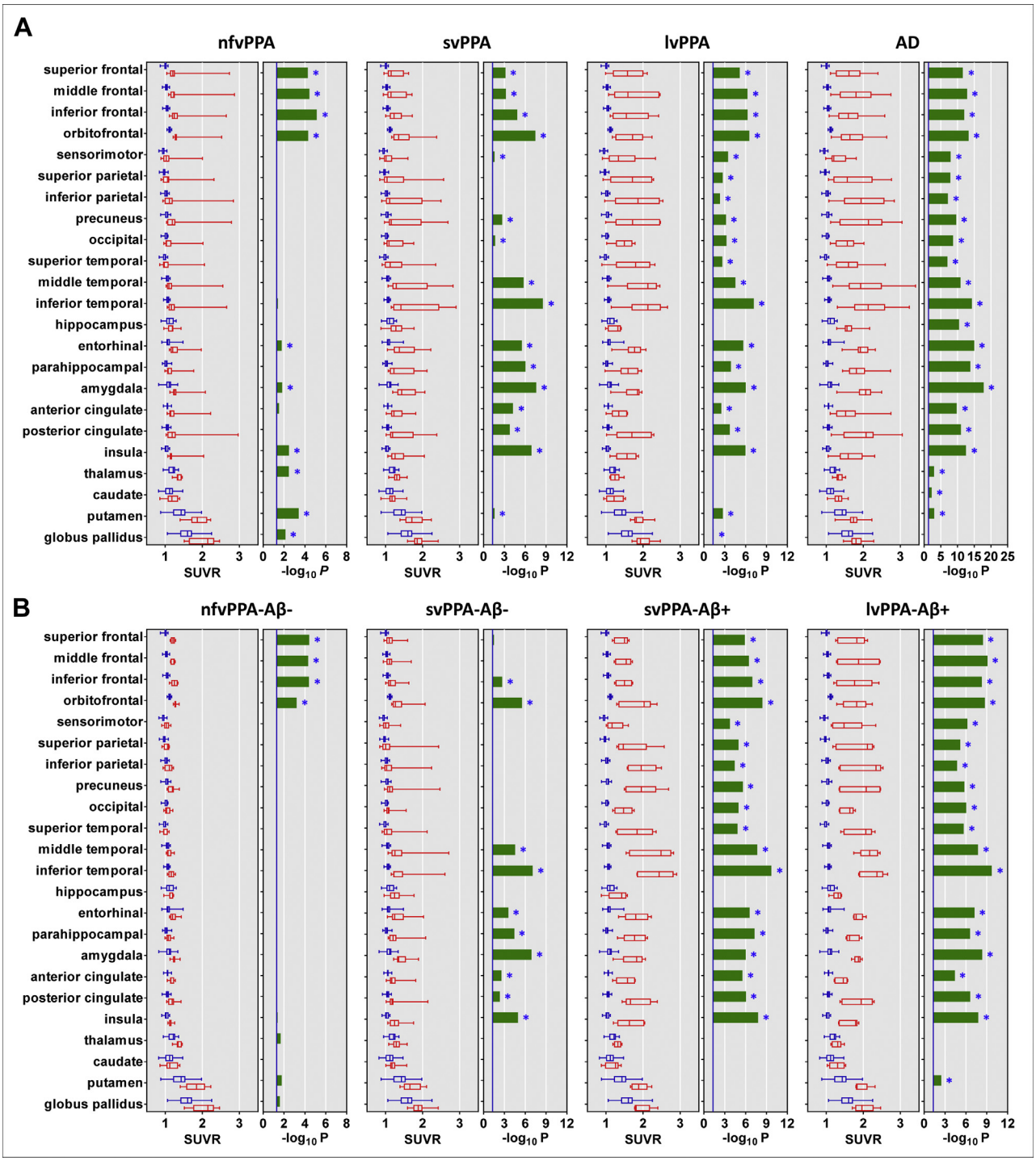

Fig. 1. Comparisons of regional ^{18}F-flortaucipir uptake values between the controls and each disease group. Regional ^{18}F-flortaucipir uptake values were compared between the controls and each diagnostic group (A) and between the controls and each subtype of PPA stratified by amyloid-positivity (B). Regional ^{18}F-flortaucipir SUVR values are presented as box-and-whisker plots (blue: HC, red: each subgroup of PPA or AD). Log-scaled *p*-values for the comparison between the controls and each disease group are presented (green bar graphs). Vertical blue lines in *p*-value charts represent *p*-value cutoffs (0.05) uncorrected for multiple comparisons. Blue asterisks represent regions that survived region-wise correction for multiple comparisons. Abbreviations: AD, Alzheimer's disease; Aβ+/-, amyloid-positivity; HC, healthy controls; lvPPA, logopenic variant PPA; nfvPPA, nonfluent variant PPA; PPA, primary progressive aphasia; svPPA, semantic variant PPA; SUVR, standardized uptake value ratio. (For interpretation of the references to color in this figure legend, the reader is referred to the Web version of this article.)

3.5. Correlation of the regional ^{18}F-flortaucipir uptake and language functions

We performed correlation analysis between language performance and regional ^{18}F-flortaucipir uptake within the nfvPPA, svPPA, and lvPPA groups and across PPA groups. However, ^{18}F-flortaucipir uptake showed no correlation with naming (BNT) and fluency (Controlled Oral Word Association Test-Semantics) after correcting for multiple comparisons (Table S5).

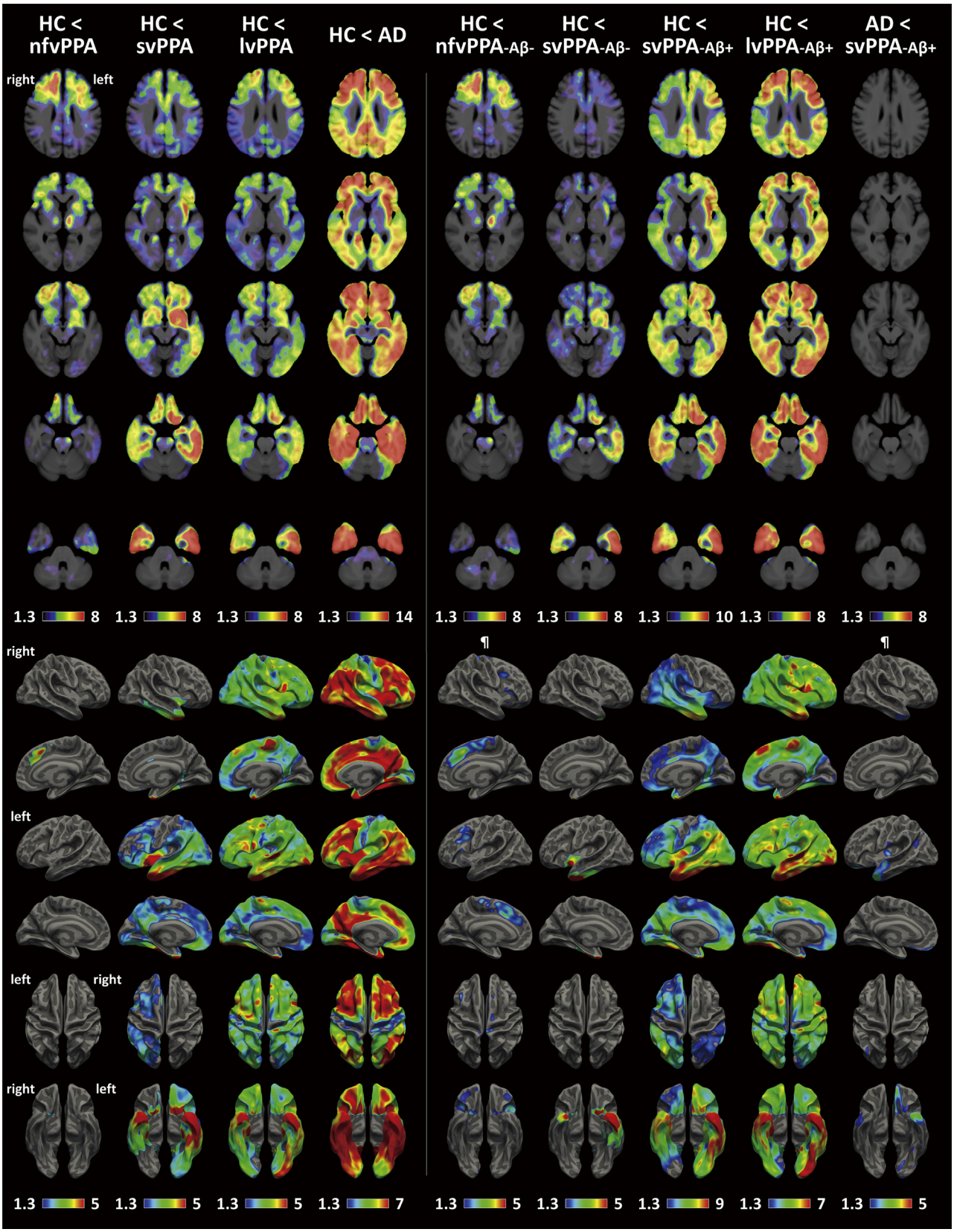

Fig. 2. Voxel-based comparisons of ^{18}F-flortaucipir PET between diagnostic groups Significance maps are projected on Axial slice view overlaid on the template magnetic resonance image (upper panel) and 3D-cortical surfaces (lower panel). Except for the comparisons marked with ¶, only the voxels or vertices that survived correction for multiple comparisons with a false discovery rate (corrected $p < 0.05$) are displayed. Color bars represent -$\log_{10}p$-values for each comparison. Due to a sizable difference in the ^{18}F-flortaucipir binding, comparisons between HC and AD or svPPA-Aβ+ (upper panel) and comparisons between HC and AD, svPPA-Aβ+, or lvPPA-Aβ+ (lower panel) used different color window for the other subgroups of PPA. Abbreviations: AD, Alzheimer's disease; Aβ+/-, amyloid-positivity; HC, healthy controls; lvPPA, logopenic variant PPA; nfvPPA, nonfluent variant PPA; PPA, primary progressive aphasia; svPPA, semantic variant PPA; SUVR, standardized uptake value ratio. (For interpretation of the references to color in this figure legend, the reader is referred to the Web version of this article.)

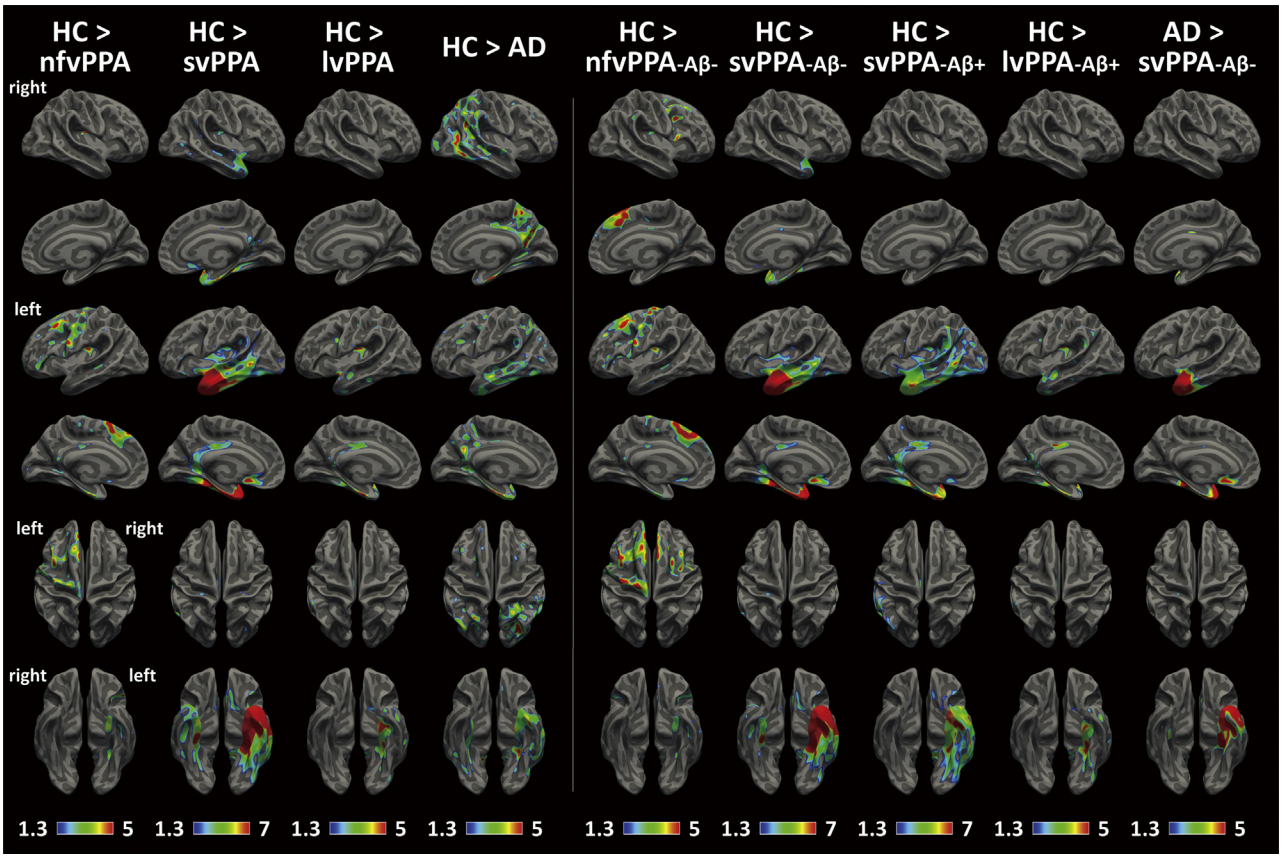

Fig. 3. Comparisons of cortical thickness between the diagnostic groups. Only the vertices that survived correction for multiple comparisons with a false discovery rate (corrected $p < 0.05$) are displayed. Color bars represent -$\log_{10}p$-values for each comparison. The comparisons between HC and svPPA (svPPA-Aβ+ or svPPA-Aβ-) used color window 1.3–7 and the other comparisons used color window 1.3–5. Abbreviations: AD, Alzheimer's disease; Aβ+/-, amyloid-positivity; HC, healthy controls; lvPPA, logopenic variant PPA; nfvPPA, nonfluent variant PPA; PPA, primary progressive aphasia; svPPA, semantic variant PPA; SUVR, standardized uptake value ratio. (For interpretation of the references to color in this figure legend, the reader is referred to the Web version of this article.)

4. Discussion

In this study, we identified distinct ^{18}F-flortaucipir uptake patterns for the subtypes of PPA. The frontal cortex and its associated subcortical white matter, and subcortical nuclei were the primary areas with increased ^{18}F-flortaucipir uptake in nfvPPA and nfvPPA-Aβ− patients. Patients with svPPA and its subgroups (svPPA-Aβ− and svPPA-Aβ+) showed increased ^{18}F-flortaucipir uptake in the widespread neocortex with clear left anterior temporal predominance. The ^{18}F-flortaucipir uptake patterns in the lvPPA and lvPPA-Aβ+ patients were more similar to the patterns shown in AD than other types of PPA, with mild predominance in the left lateral temporal cortex. Regions with predominantly increased uptake in each PPA type corresponded to the regions showing cortical thinning. Language performance did not correlate with regional ^{18}F-flortaucipir uptake in our patients with PPA. Lack of correlation between language performance and ^{18}F-flortaucipir uptake in the distinct language center where the tracer binding was prominent could be due to pathological heterogeneity.

4.1. Nonfluent/agrammatic PPA

Voxel-based morphometry studies in nfvPPA have consistently shown gray matter atrophy in the posterior and inferior frontal, and insula cortices, predominantly in the left side (Gorno-Tempini et al., 2004; Santos-Santos et al., 2016; Whitwell et al., 2010; Wilson et al., 2010). Similar areas were affected by cortical thinning (Rogalski et al., 2011) and by hypometabolism in nfvPPA compared to the controls (Josephs et al., 2010; Rabinovici et al., 2008). Structural changes in these areas are closely related to motor speech and syntactic processes, which are dysfunctional in nfvPPA (Wilson et al., 2010). As expected by these structural and functional imaging studies, the widespread frontal cortex showed increased ^{18}F-flortaucipir uptake in the patients with nfvPPA, even after the exclusion of 2 nfvPPA-Aβ+ patients.

It is interesting to note that the ^{18}F-flortaucipir uptake was also highly increased in the frontal subcortical white matter in both nfvPPA and nfvPPA-Aβ- patients (Fig. 2). Subcortical structures such as the thalamus and basal ganglia also showed mildly increased uptake. When previous neuropathological studies reported by 4 different centers were collectively analyzed (Josephs et al., 2006; Knibb et al., 2006; Mesulam et al., 2008; Rohrer et al., 2011), corticobasal degeneration (CBD) was found to be the most frequent pathological diagnosis in 43% of patients with nfvPPA with FTLD-tau pathology and was followed by progressive supranuclear palsy (PSP) in 32% and Pick's disease in 23%. In addition to gray matter, tau pathology in white matter is prominently observed in the CBD as numerous threads and oligodendroglial inclusions (Dickson et al., 2002; Ling et al., 2016). Similar white matter tau pathology also exists in PSP and Pick's disease (de Silva et al., 2006; Williams et al., 2007; Zhukareva et al., 2002). Both PSP and CBD are also characterized by prominent tau pathology in the subcortical gray matter structures such as the striatum, pallidum, subthalamic nucleus, and substantia nigra (Dickson et al., 2002; Williams et al., 2007). Recent ^{18}F-flortaucipir PET studies demonstrated predominantly increased subcortical white and gray matter in PSP and corticobasal syndrome (Cho et al., 2017;

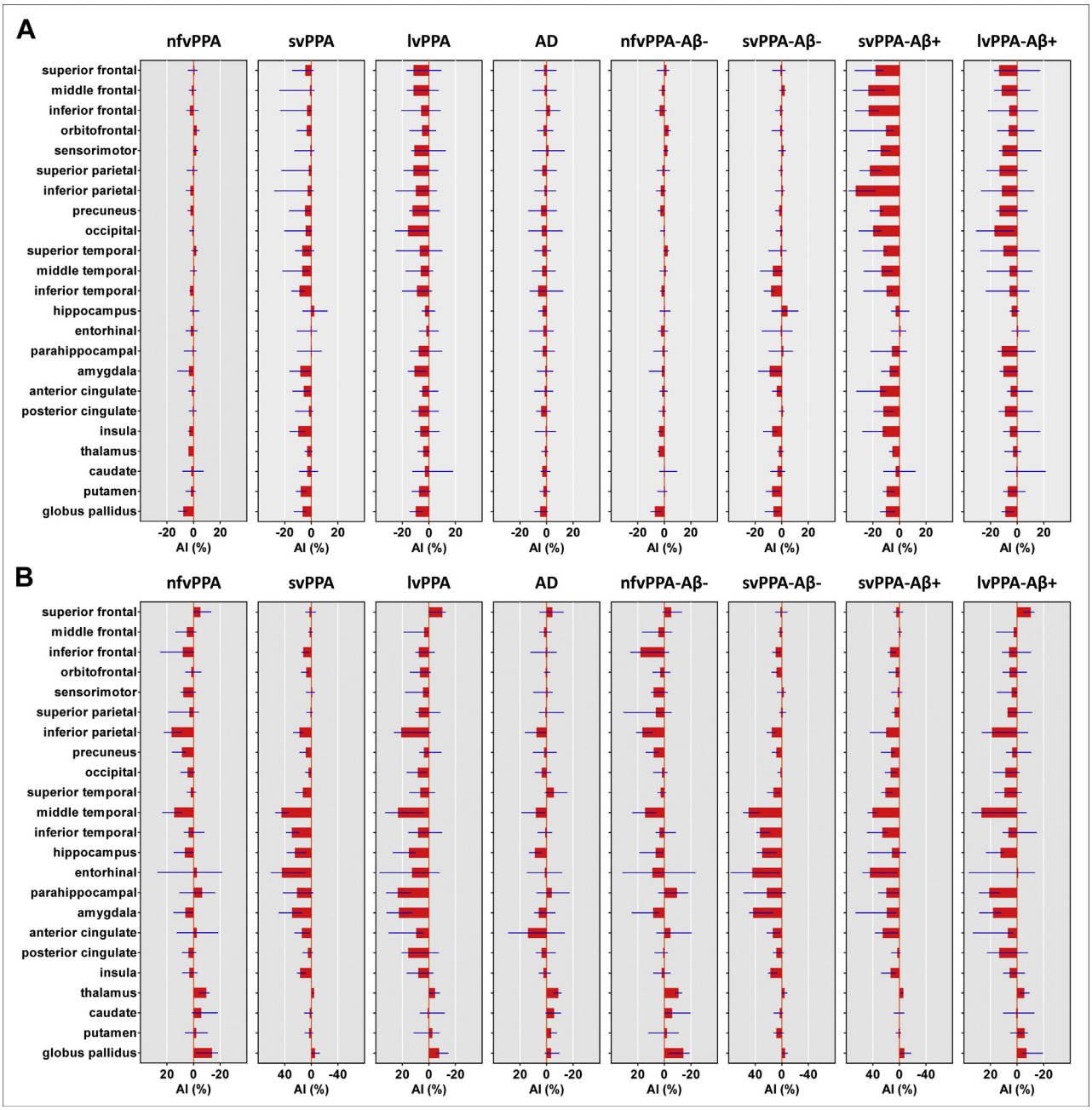

Fig. 4. Regional asymmetry indexes for ^{18}F-flortaucipir uptake (A) and volume (B) in each diagnostic group. Horizontal red bars and overlying horizontal blue lines represent median and interquartile ranges of uptake values or volumes. Asymmetry index (AI) was calculated with the formula (R−L)/(R + L) × 200 (%), and the negative AI of ^{18}F-flortaucipir uptake (A), indicating greater uptake in the left side than the right side. Conversely, the positive AI for regional volume (B) indicates greater atrophy in the left side than the right side. Abbreviations: AD, Alzheimer's disease; Aβ+/-, amyloid-positivity; HC, healthy controls; lvPPA, logopenic variant PPA; nfvPPA, nonfluent variant PPA; PPA, primary progressive aphasia; svPPA, semantic variant PPA; SUVR, standardized uptake value ratio. (For interpretation of the references to color in this figure legend, the reader is referred to the Web version of this article.)

Passamonti et al., 2017). In addition, one ^{18}F-flortaucipir PET study showed increased binding throughout the prefrontal white matter and in subcortical gray matter structures in 13 patients with nfvPPA (Josephs et al., 2018), which was consistent with our results. Therefore, the subcortical preference of ^{18}F-flortaucipir binding in nfvPPA can be explained by tau pathology, but the extent of binding was much less than that in AD due to weak binding affinity of ^{18}F-flortaucipir to FTLD-tau, as shown in an autoradiography study of postmortem tissues (Lowe et al., 2016). However, the possibility remains that the binding observed in nfvPPA could be nonspecific off-target binding.

Unexpectedly, in our patients with nfvPPA and nfvPPA-Aβ-, we found no asymmetry of cortical ^{18}F-flortaucipir uptake, while there was left dominant volume atrophy in the inferior parietal, precuneus, and middle temporal cortices. Although a previous study of patients with nfvPPA has shown evidence of bilateral structural changes in frontal regions (Cope et al., 2017), the mechanism responsible for this discrepancy remains unknown. A further ^{18}F-flortaucipir PET study in different patients with nfvPPA would be required to help determine whether this discrepancy can be replicated.

4.2. Semantic variant PPA

In patients with svPPA, volume atrophy (Gorno-Tempini et al., 2004; Whitwell et al., 2010; Wilson et al., 2010), cortical thinning (Rogalski et al., 2011), and hypometabolism (Acosta-Cabronero et al., 2011; Rabinovici et al., 2008) in the anterior temporal cortex, predominantly in the left side, have been consistently observed in previous neuroimaging studies. The left anterior temporal cortex plays an important role in the integrity of semantic memory function (Patterson et al., 2007), and structural change in the left anterior temporal cortex impairs retrieval of lexical contents (Wilson et al., 2010). Therefore, the left anterior temporal cortex is a key area for the development of svPPA.

TDP43 type C is the major pathological substrate for svPPA (Rohrer et al., 2011) and has been identified in over 75% of patients with svPPA in postmortem studies (Chare et al., 2014; Harris et al., 2013; Josephs et al., 2006; Kertesz et al., 2005; Mesulam et al., 2008; Rohrer et al., 2011). FTLD-tau and AD tau pathology could be found only in 15% and 10% of patients with svPPA, respectively. Therefore, we may expect that tau PET is not the most appropriate tool for observing the pathology in svPPA-Aβ- patients and is only of limited utility for showing AD tau pathology in svPPA-Aβ+. The svPPA-Aβ+ patients showed asymmetrically increased uptake in the lateral and medial temporal, cingulate, frontal, and parieto-occipital cortices, most prominently in the left anterior temporal cortex. However, contrary to our expectations, we found highly increased ^{18}F-flortaucipir uptake in the inferior frontal, orbito-frontal, lateral and medial temporal, cingulate and insula cortices, most prominently in the left anterior temporal cortex. Moreover, all svPPA-Aβ− patients showed at least weakly increased ^{18}F-flortaucipir uptake in the anterior inferior temporal cortex. Similar to our results, a recent ^{18}F-flortaucipir PET study in 7 patients with svPPA (4 svPPA-Aβ− and 3 unknown for Aβ-negativity) has shown asymmetrically increased ^{18}F-flortaucipir binding in the anterior temporal cortex (Bevan-Jones et al., 2017). Another ^{18}F-flortaucipir PET study in 7 patients with svPPA (5 svPPA-Aβ−, one svPPA-Aβ+, and one unknown for Aβ-negativity) and patients with 13 svPPA replicated this finding (Josephs et al., 2018; Makaretz et al., 2018). Considering the small proportion of FTLD-tau pathology in svPPA, it seems unlikely that ^{18}F-flortaucipir bound to tau pathology. One possible explanation for this unexpected ^{18}F-flortaucipir binding is weak affinity to TDP43. Although 2 autoradiography studies of postmortem tissue showed no ^{18}F-flortaucipir binding to TDP43 pathology (Marquie et al., 2015, 2017), weak ^{18}F-flortaucipir binding to TDP43 was reported by another autoradiography study (Lowe et al., 2016). Binding to MAO-B expressed by reactive astrocytes has been suggested as an alternative mechanism (Bevan-Jones et al., 2017). However, these observations need to be further investigated in a postmortem study.

Interestingly, both svPPA-Aβ− and svPPA-Aβ+ groups shared cortical thinning patterns in the left anterior temporal cortex, for which cortical thinning was more prominent in the svPPA-Aβ− group than in the svPPA-Aβ+ group. Considering that there was increased ^{18}F-flortaucipir uptake in the svPPA-Aβ+ patients than in svPPA-Aβ-, cortical atrophy in svPPA-Aβ− can be explained only partly by ^{18}F-flortaucipir uptake, while TDP pathology and resulting neurodegeneration might be closer related.

4.3. Logopenic variant PPA

AD pathology is found in 54%–77% of patients with lvPPA (Chare et al., 2014; Harris et al., 2013; Josephs et al., 2006; Kertesz et al., 2005; Mesulam et al., 2008; Rohrer et al., 2011). Therefore, distribution patterns of volume atrophy (Hu et al., 2010; Madhavan et al., 2013; Wilson et al., 2010), cortical thinning (Rogalski et al., 2011), and hypometabolism (Josephs et al., 2010; Krishnan et al., 2017; Madhavan et al., 2013; Rabinovici et al., 2008) are similar to patterns shown in AD. Previous structural and functional imaging studies have consistently reported that the left temporoparietal cortex is the most predominantly involved area.

Prominently increased ^{18}F-flortaucipir binding in the lateral tempoparietal cortex was reported in 5 patients with lvPPA including 4 lvPPA-Aβ+ patients (Ossenkoppele et al., 2016). In addition, recent PET with ^{18}F-flortaucipir studies have shown consistent cortical binding patterns in the left-side lateralized temporo-parietal cortices (Josephs et al., 2018; Nasrallah et al., 2018; Xia et al., 2017). Josephs et al. reported that patients with lvPPA had significantly increased ^{18}F-flortaucipir uptake compared to the other variants as well as controls, and therefore ^{18}F-flortaucipir uptake characteristics could provide a useful method to distinguish between the subtypes of PPA (Josephs et al., 2018). Although our results were consistent for comparisons with NC, there was no statistical significance in comparisons between the variants, which may be due to the small the sample sizes in our study.

Likewise, lvPPA-Aβ+ patients in our study showed patterns of increased ^{18}F-flortaucipir uptake and cortical thinning very similar to that of AD apart from less prominent uptake and cortical thinning in the medial temporal cortex, especially in the hippocampus. In addition, it is noteworthy that the left-side asymmetry of ^{18}F-flortaucipir uptake was demonstrated in 4 lvPPA-Aβ+ patients, although patients with AD did not show clear asymmetry. An exceptional pattern of right-dominant ^{18}F-flortaucipir uptake and hypometabolism and left dominant Aβ accumulation was previously reported in one right-handed lvPPA-Aβ+ patient (Jang et al., 2016). Language presentation in AD may be attributable to asymmetric involvement of the dominant temporo-parietal cortex.

4.4. Miscellaneous patients with PPA

Two nfvPPA-Aβ+ patients and one lvPPA-Aβ− patient were not included in the statistical analysis after stratification for Aβ-positivity due to the small numbers available for analysis. When we investigated the range of prevalence of the pathologies, a proportion of AD tau pathology was 0%–41% in the patients with nfvPPA (Harris et al., 2013; Josephs et al., 2014; Kertesz et al., 2005; Knibb et al., 2006; Mesulam et al., 2008; Rohrer et al., 2010, 2011), the amyloid-positive nfvPPA patient in our study (2/13, 83%) is consistent with other studies. One nfvPPA-Aβ+ patient (female patient with age 59 years; nfvPPA-Aβ+ #2 in Fig. S3) showed highly increased ^{18}F-flortaucipir uptake in the diffuse frontotemporoparietal cortex without clear asymmetry, relatively sparing the primary cortex, as for AD. The other nfvPPA-Aβ+ patient (male patient, age 68 years; nfvPPA-Aβ+ #1 in Fig. S3) did not show highly increased ^{18}F-flortaucipir uptake, as with the other PPA-Aβ+ groups. Slightly increased uptake in the frontal cortex and subcortical structures was similar to the pattern shown in the nfvPPA-Aβ− patients, and it is possible that Aβ accumulation was an incidental finding. One lvPPA-Aβ− patient (female patient aged 59 years; Fig. S3) showed weakly elevated uptake in the left lateral frontotemporal cortex. A voxel-based morphometry study showed that volume atrophy was prominent in the fronto-temporal cortex in lvPPA-Aβ− patients and in the temporoparietal cortex in lvPPA-Aβ+ patients (Hu et al., 2010). Although the underlying pathology cannot be determined in this lvPPA-Aβ- patient, the ^{18}F-flortaucipir uptake pattern was similar to the atrophic areas found in the lvPPA-Aβ- patients.

4.5. Limitations

This study was limited by the absence of neuropathological and cerebrospinal fluid observations, which would be helpful for the

diagnosis of non-AD PPA patients and enable the extraction of tau-specific uptake patterns from the patients with PPA with heterogeneous pathology. In addition, unknown off-target binding such as with MAO-B should be considered (Bevan-Jones et al., 2017). Second, quantitative data for various components of language functions were not available to us. This limited further investigation of the relationships between specific language components and regional ^{18}F-flortaucipir binding. Third, the majority of PPA is sporadic, but some genetic forms of FTLD have been recognized in patients with PPA including microtubule-associated protein tau (*MAPT*), progranulin (*PGRN*), and the chromosome 9 open reading frame 72 protein (*C9orf72*) genes (Grossman, 2010). Genome analysis was also absent. Fourth, although the nonparametric analysis method was used, this study enrolled a small number of patients with PPA, limiting the generalizability of our findings. In addition, although 3 of 5 svPPA-Aβ+ patients had low Mini-Mental State Examination scores, less than 3, due to a very poor comprehension of words at the time of brain imaging, they were eligible for svPPA and their clinical diagnosis was unchanged for an average of 24 months during the observational period. Finally, a greater number of patients with minor PPA subtypes such as nfvPPA-Aβ+ or lvPPA-Aβ− may have provided additional information regarding the distinct ^{18}F-flortaucipir binding patterns related to specific language dysfunction.

5. Conclusions

In summary, the uptake patterns of ^{18}F-flortaucipir and cortical atrophy were distinct and corresponded to areas related to the specific language functions that are distinctly impaired in each subtype of PPA; increased uptake in the frontal cortex and underlying white matter, and subcortical gray matter in nfvPPA, in the left anterior temporal cortex in svPPA, and in the left temporoparietal cortex in lvPPA. However, because pathological heterogeneities exist in such patients, the interpretation of ^{18}F-flortaucipir uptake and the possibility of unknown “off-target” binding should be considered in any interpretation of our findings.

Disclosure

The authors report no disclosures relevant to the article.

Acknowledgements

This study was financially supported by a faculty research grant of Yonsei University College of Medicine, South Korea for (2018-32-0036), National Research Foundation of Korea, South Korea grant funded by the Korean government (MSIP) (No. 2015R1C1A2A01054507, 2017R1A2B2006694, and 2017R1A2B2005081), and a grant of the Korea Health Technology R&D Project through the Korea Health Industry Development Institute, South Korea (KHIDI), funded by the Ministry of Health & Welfare, Republic of Korea (grant number: HI18C1159 and HI18C1629).

Appendix A. Supplementary data

Supplementary data associated with this article can be found, in the online version, at https://doi.org/10.1016/j.neurobiolaging.2018.11.017.

References

Acosta-Cabronero, J., Patterson, K., Fryer, T.D., Hodges, J.R., Pengas, G., Williams, G.B., Nestor, P.J., 2011. Atrophy, hypometabolism and white matter abnormalities in semantic dementia tell a coherent story. Brain 134, 2025–2035.

Benjamini, Y., Hochberg, Y., 1995. Controlling the false discovery rate: a practical and powerful approach to multiple testing. J. R. Stat. Soc. B Stat. Methodol. 57, 289–300.

Bevan-Jones, W.R., Cope, T.E., Jones, P.S., Passamonti, L., Hong, Y.T., Fryer, T.D., Arnold, R., Allinson, K.S.J., Coles, J.P., Aigbirhio, F.I., Patterson, K., O'Brien, J.T., Rowe, J.B., 2017. [(18)F]AV-1451 binding in vivo mirrors the expected distribution of TDP-43 pathology in the semantic variant of primary progressive aphasia. J. Neurol. Neurosurg. Psychiatry 89, 1032–1037.

Chare, L., Hodges, J.R., Leyton, C.E., McGinley, C., Tan, R.H., Kril, J.J., Halliday, G.M., 2014. New criteria for frontotemporal dementia syndromes: clinical and pathological diagnostic implications. J. Neurol. Neurosurg. Psychiatry 85, 865–870.

Cho, H., Baek, M.S., Choi, J.Y., Lee, S.H., Kim, J.S., Ryu, Y.H., Lee, M.S., Lyoo, C.H., 2017. 18F-AV-1451 binds to motor-related subcortical gray and white matter in corticobasal syndrome. Neurology 89, 1170–1178.

Cho, H., Choi, J.Y., Hwang, M.S., Kim, Y.J., Lee, H.M., Lee, H.S., Lee, J.H., Ryu, Y.H., Lee, M.S., Lyoo, C.H., 2016. In vivo cortical spreading pattern of tau and amyloid in the Alzheimer disease spectrum. Ann. Neurol. 80, 247–258.

Christensen, K.J., Multhaup, K.S., Nordstrom, S., Voss, K., 1991. A cognitive battery for dementia: development and measurement characteristics. Psychol. Assess. 3, 168.

Cope, T.E., Wilson, B., Robson, H., Drinkall, R., Dean, L., Grube, M., Jones, P.S., Patterson, K., Griffiths, T.D., Rowe, J.B., Petkov, C.I., 2017. Artificial grammar learning in vascular and progressive non-fluent aphasias. Neuropsychologia 104, 201–213.

de Silva, R., Lashley, T., Strand, C., Shiarli, A.M., Shi, J., Tian, J., Bailey, K.L., Davies, P., Bigio, E.H., Arima, K., Iseki, E., Murayama, S., Kretzschmar, H., Neumann, M., Lippa, C., Halliday, G., MacKenzie, J., Ravid, R., Dickson, D., Wszolek, Z., Iwatsubo, T., Pickering-Brown, S.M., Holton, J., Lees, A., Revesz, T., Mann, D.M., 2006. An immunohistochemical study of cases of sporadic and inherited frontotemporal lobar degeneration using 3R- and 4R-specific tau monoclonal antibodies. Acta Neuropathol. 111, 329–340.

Desikan, R.S., Segonne, F., Fischl, B., Quinn, B.T., Dickerson, B.C., Blacker, D., Buckner, R.L., Dale, A.M., Maguire, R.P., Hyman, B.T., Albert, M.S., Killiany, R.J., 2006. An automated labeling system for subdividing the human cerebral cortex on MRI scans into gyral based regions of interest. Neuroimage 31, 968–980.

Dickson, D.W., Bergeron, C., Chin, S.S., Duyckaerts, C., Horoupian, D., Ikeda, K., Jellinger, K., Lantos, P.L., Lippa, C.F., Mirra, S.S., Tabaton, M., Vonsattel, J.P., Wakabayashi, K., Litvan, I., Office of Rare Diseases of the National Institutes of Health, 2002. Office of rare diseases neuropathologic criteria for corticobasal degeneration. J. Neuropathol. Exp. Neurol. 61, 935–946.

Fischl, B., Salat, D.H., Busa, E., Albert, M., Dieterich, M., Haselgrove, C., van der Kouwe, A., Killiany, R., Kennedy, D., Klaveness, S., Montillo, A., Makris, N., Rosen, B., Dale, A.M., 2002. Whole brain segmentation: automated labeling of neuroanatomical structures in the human brain. Neuron 33, 341–355.

Fischl, B., van der Kouwe, A., Destrieux, C., Halgren, E., Segonne, F., Salat, D.H., Busa, E., Seidman, L.J., Goldstein, J., Kennedy, D., Caviness, V., Makris, N., Rosen, B., Dale, A.M., 2004. Automatically parcellating the human cerebral cortex. Cereb. Cortex. 14, 11–22.

Gorno-Tempini, M.L., Dronkers, N.F., Rankin, K.P., Ogar, J.M., Phengrasamy, L., Rosen, H.J., Johnson, J.K., Weiner, M.W., Miller, B.L., 2004. Cognition and anatomy in three variants of primary progressive aphasia. Ann. Neurol. 55, 335–346.

Gorno-Tempini, M.L., Hillis, A.E., Weintraub, S., Kertesz, A., Mendez, M., Cappa, S.F., Ogar, J.M., Rohrer, J.D., Black, S., Boeve, B.F., Manes, F., Dronkers, N.F., Vandenberghe, R., Rascovsky, K., Patterson, K., Miller, B.L., Knopman, D.S., Hodges, J.R., Mesulam, M.M., Grossman, M., 2011. Classification of primary progressive aphasia and its variants. Neurology 76, 1006–1014.

Grossman, M., 2010. Primary progressive aphasia: clinicopathological correlations. Nat. Rev. Neurol. 6, 88–97.

Harris, J.M., Gall, C., Thompson, J.C., Richardson, A.M., Neary, D., du Plessis, D., Pal, P., Mann, D.M., Snowden, J.S., Jones, M., 2013. Classification and pathology of primary progressive aphasia. Neurology 81, 1832–1839.

Hu, W.T., McMillan, C., Libon, D., Leight, S., Forman, M., Lee, V.M., Trojanowski, J.Q., Grossman, M., 2010. Multimodal predictors for Alzheimer disease in nonfluent primary progressive aphasia. Neurology 75, 595–602.

Jang, Y.K., Park, S., Kim, H.J., Cho, H., Lyoo, C.H., Seo, S.W., Na, D.L., 2016. A dextral primary progressive aphasia patient with right dominant hypometabolism and tau accumulation and left dominant amyloid accumulation. Case Rep. Neurol. 8, 78–86.

Johnson, K.A., Schultz, A., Betensky, R.A., Becker, J.A., Sepulcre, J., Rentz, D., Mormino, E., Chhatwal, J., Amariglio, R., Papp, K., Marshall, G., Albers, M., Mauro, S., Pepin, L., Alverio, J., Judge, K., Philiossaint, M., Shoup, T., Yokell, D., Dickerson, B., Gomez-Isla, T., Hyman, B., Vasdev, N., Sperling, R., 2016. Tau positron emission tomographic imaging in aging and early Alzheimer disease. Ann. Neurol. 79, 110–119.

Josephs, K.A., Duffy, J.R., Fossett, T.R., Strand, E.A., Claassen, D.O., Whitwell, J.L., Peller, P.J., 2010. Fluorodeoxyglucose F18 positron emission tomography in progressive apraxia of speech and primary progressive aphasia variants. Arch. Neurol. 67, 596–605.

Josephs, K.A., Duffy, J.R., Strand, E.A., Machulda, M.M., Vemuri, P., Senjem, M.L., Perkerson, R.B., Baker, M.C., Lowe, V., Jack Jr., C.R., Rademakers, R., Whitwell, J.L., 2014. Progranulin-associated PiB-negative logopenic primary progressive aphasia. J. Neurol. 261, 604–614.

Josephs, K.A., Duffy, J.R., Strand, E.A., Whitwell, J.L., Layton, K.F., Parisi, J.E., Hauser, M.F., Witte, R.J., Boeve, B.F., Knopman, D.S., Dickson, D.W., Jack Jr., C.R.,

Petersen, R.C., 2006. Clinicopathological and imaging correlates of progressive aphasia and apraxia of speech. Brain 129, 1385–1398.
Josephs, K.A., Martin, P.R., Botha, H., Schwarz, C.G., Duffy, J.R., Clark, H.M., Machulda, M.M., Graff-Radford, J., Weigand, S.D., Senjem, M.L., Utianski, R.L., Drubach, D.A., Boeve, B.F., Jones, D.T., Knopman, D.S., Petersen, R.C., Jack Jr., C.R., Lowe, V.J., Whitwell, J.L., 2018. [(18) F]AV-1451 tau-PET and primary progressive aphasia. Ann. Neurol. 83, 599–611.
Kertesz, A., McMonagle, P., Blair, M., Davidson, W., Munoz, D.G., 2005. The evolution and pathology of frontotemporal dementia. Brain 128, 1996–2005.
Knibb, J.A., Xuereb, J.H., Patterson, K., Hodges, J.R., 2006. Clinical and pathological characterization of progressive aphasia. Ann. Neurol. 59, 156–165.
Krishnan, K., Machulda, M.M., Whitwell, J.L., Butts, A.M., Duffy, J.R., Strand, E.A., Senjem, M.L., Spychalla, A.J., Jack, C.R., Lowe, V.J., Josephs, K.A., 2017. Varying degrees of temporoparietal hypometabolism on FDG-PET reveal amyloid-positive logopenic primary progressive aphasia is not a homogeneous clinical entity. J. Alzheimers Dis. 55, 1019–1029.
Ling, H., Kovacs, G.G., Vonsattel, J.P., Davey, K., Mok, K.Y., Hardy, J., Morris, H.R., Warner, T.T., Holton, J.L., Revesz, T., 2016. Astrogliopathy predominates the earliest stage of corticobasal degeneration pathology. Brain 139, 3237–3252.
Lowe, V.J., Curran, G., Fang, P., Liesinger, A.M., Josephs, K.A., Parisi, J.E., Kantarci, K., Boeve, B.F., Pandey, M.K., Bruinsma, T., Knopman, D.S., Jones, D.T., Petrucelli, L., Cook, C.N., Graff-Radford, N.R., Dickson, D.W., Petersen, R.C., Jack Jr., C.R., Murray, M.E., 2016. An autoradiographic evaluation of AV-1451 Tau PET in dementia. Acta Neuropathol. Commun. 4, 58.
Madhavan, A., Whitwell, J.L., Weigand, S.D., Duffy, J.R., Strand, E.A., Machulda, M.M., Tosakulwong, N., Senjem, M.L., Gunter, J.L., Lowe, V.J., Petersen, R.C., Jack Jr., C.R., Josephs, K.A., 2013. FDG PET and MRI in logopenic primary progressive aphasia versus dementia of the Alzheimer's type. PLoS One 8, e62471.
Makaretz, S.J., Quimby, M., Collins, J., Makris, N., McGinnis, S., Schultz, A., Vasdev, N., Johnson, K.A., Dickerson, B.C., 2018. Flortaucipir tau PET imaging in semantic variant primary progressive aphasia. J. Neurol. Neurosurg. Psychiatry 89, 1024–1031.
Marquie, M., Normandin, M.D., Meltzer, A.C., Siao Tick Chong, M., Andrea, N.V., Anton-Fernandez, A., Klunk, W.E., Mathis, C.A., Ikonomovic, M.D., Debnath, M., Bien, E.A., Vanderburg, C.R., Costantino, I., Makaretz, S., DeVos, S.L., Oakley, D.H., Gomperts, S.N., Growdon, J.H., Domoto-Reilly, K., Lucente, D., Dickerson, B.C., Frosch, M.P., Hyman, B.T., Johnson, K.A., Gomez-Isla, T., 2017. Pathological correlations of [F-18]-AV-1451 imaging in non-alzheimer tauopathies. Ann. Neurol. 81, 117–128.
Marquie, M., Normandin, M.D., Vanderburg, C.R., Costantino, I.M., Bien, E.A., Rycyna, L.G., Klunk, W.E., Mathis, C.A., Ikonomovic, M.D., Debnath, M.L., Vasdev, N., Dickerson, B.C., Gomperts, S.N., Growdon, J.H., Johnson, K.A., Frosch, M.P., Hyman, B.T., Gomez-Isla, T., 2015. Validating novel tau positron emission tomography tracer [F-18]-AV-1451 (T807) on postmortem brain tissue. Ann. Neurol. 78, 787–800.
McKhann, G.M., Knopman, D.S., Chertkow, H., Hyman, B.T., Jack Jr., C.R., Kawas, C.H., Klunk, W.E., Koroshetz, W.J., Manly, J.J., Mayeux, R., Mohs, R.C., Morris, J.C., Rossor, M.N., Scheltens, P., Carrillo, M.C., Thies, B., Weintraub, S., Phelps, C.H., 2011. The diagnosis of dementia due to Alzheimer's disease: recommendations from the national institute on aging-Alzheimer's Association workgroups on diagnostic guidelines for Alzheimer's disease. Alzheimers Dement. 7, 263–269.
Mesulam, M., Wicklund, A., Johnson, N., Rogalski, E., Leger, G.C., Rademaker, A., Weintraub, S., Bigio, E.H., 2008. Alzheimer and frontotemporal pathology in subsets of primary progressive aphasia. Ann. Neurol. 63, 709–719.
Mesulam, M.M., 2001. Primary progressive aphasia. Ann. Neurol. 49, 425–432.
Nasrallah, I.M., Chen, Y.J., Hsieh, M.K., Phillips, J.S., Ternes, K., Stockbower, G.E., Sheline, Y., McMillan, C.T., Grossman, M., Wolk, D.A., 2018. (18)F-Flortaucipir PET/MRI correlations in nonamnestic and amnestic variants of alzheimer disease. J. Nucl. Med. 59, 299–306.
Ossenkoppele, R., Schonhaut, D.R., Scholl, M., Lockhart, S.N., Ayakta, N., Baker, S.L., O'Neil, J.P., Janabi, M., Lazaris, A., Cantwell, A., Vogel, J., Santos, M., Miller, Z.A., Bettcher, B.M., Vossel, K.A., Kramer, J.H., Gorno-Tempini, M.L., Miller, B.L., Jagust, W.J., Rabinovici, G.D., 2016. Tau PET patterns mirror clinical and neuroanatomical variability in Alzheimer's disease. Brain 139, 1551–1567.
Passamonti, L., Vazquez Rodriguez, P., Hong, Y.T., Allinson, K.S., Williamson, D., Borchert, R.J., Sami, S., Cope, T.E., Bevan-Jones, W.R., Jones, P.S., Arnold, R., Surendranathan, A., Mak, E., Su, L., Fryer, T.D., Aigbirhio, F.I., O'Brien, J.T., Rowe, J.B., 2017. 18F-AV-1451 positron emission tomography in Alzheimer's disease and progressive supranuclear palsy. Brain 140, 781–791.
Patterson, K., Nestor, P.J., Rogers, T.T., 2007. Where do you know what you know? The representation of semantic knowledge in the human brain. Nat. Rev. Neurosci. 8, 976–987.
Quade, D., 1967. Rank analysis of covariance. J. Am. Stat. Assoc. 62, 1187–1200.
Rabinovici, G.D., Jagust, W.J., Furst, A.J., Ogar, J.M., Racine, C.A., Mormino, E.C., O'Neil, J.P., Lal, R.A., Dronkers, N.F., Miller, B.L., Gorno-Tempini, M.L., 2008. Abeta amyloid and glucose metabolism in three variants of primary progressive aphasia. Ann. Neurol. 64, 388–401.
Rogalski, E., Cobia, D., Harrison, T.M., Wieneke, C., Weintraub, S., Mesulam, M.M., 2011. Progression of language decline and cortical atrophy in subtypes of primary progressive aphasia. Neurology 76, 1804–1810.
Rohrer, J.D., Crutch, S.J., Warrington, E.K., Warren, J.D., 2010. Progranulin-associated primary progressive aphasia: a distinct phenotype? Neuropsychologia 48, 288–297.
Rohrer, J.D., Lashley, T., Schott, J.M., Warren, J.E., Mead, S., Isaacs, A.M., Beck, J., Hardy, J., de Silva, R., Warrington, E., Troakes, C., Al-Sarraj, S., King, A., Borroni, B., Clarkson, M.J., Ourselin, S., Holton, J.L., Fox, N.C., Revesz, T., Rossor, M.N., Warren, J.D., 2011. Clinical and neuroanatomical signatures of tissue pathology in frontotemporal lobar degeneration. Brain 134, 2565–2581.
Santos-Santos, M.A., Mandelli, M.L., Binney, R.J., Ogar, J., Wilson, S.M., Henry, M.L., Hubbard, H.I., Meese, M., Attygalle, S., Rosenberg, L., Pakvasa, M., Trojanowski, J.Q., Grinberg, L.T., Rosen, H., Boxer, A.L., Miller, B.L., Seeley, W.W., Gorno-Tempini, M.L., 2016. Features of patients with nonfluent/agrammatic primary progressive aphasia with underlying progressive supranuclear palsy pathology or corticobasal degeneration. JAMA Neurol. 73, 733–742.
Smith, R., Puschmann, A., Scholl, M., Ohlsson, T., van Swieten, J., Honer, M., Englund, E., Hansson, O., 2016. 18F-AV-1451 tau PET imaging correlates strongly with tau neuropathology in MAPT mutation carriers. Brain 139, 2372–2379.
Thomas, B.A., Erlandsson, K., Modat, M., Thurfjell, L., Vandenberghe, R., Ourselin, S., Hutton, B.F., 2011. The importance of appropriate partial volume correction for PET quantification in Alzheimer's disease. Eur. J. Nucl. Med. Mol. Imaging 38, 1104–1119.
Villemagne, V.L., Ong, K., Mulligan, R.S., Holl, G., Pejoska, S., Jones, G., O'Keefe, G., Ackerman, U., Tochon-Danguy, H., Chan, J.G., Reininger, C.B., Fels, L., Putz, B., Rohde, B., Masters, C.L., Rowe, C.C., 2011. Amyloid imaging with (18)F-florbetaben in Alzheimer disease and other dementias. J. Nucl. Med. 52, 1210–1217.
Whitwell, J.L., Avula, R., Senjem, M.L., Kantarci, K., Weigand, S.D., Samikoglu, A., Edmonson, H.A., Vemuri, P., Knopman, D.S., Boeve, B.F., Petersen, R.C., Josephs, K.A., Jack Jr., C.R., 2010. Gray and white matter water diffusion in the syndromic variants of frontotemporal dementia. Neurology 74, 1279–1287.
Williams, D.R., Holton, J.L., Strand, C., Pittman, A., de Silva, R., Lees, A.J., Revesz, T., 2007. Pathological tau burden and distribution distinguishes progressive supranuclear palsy-parkinsonism from Richardson's syndrome. Brain 130, 1566–1576.
Wilson, S.M., Henry, M.L., Besbris, M., Ogar, J.M., Dronkers, N.F., Jarrold, W., Miller, B.L., Gorno-Tempini, M.L., 2010. Connected speech production in three variants of primary progressive aphasia. Brain 133, 2069–2088.
Xia, C., Makaretz, S.J., Caso, C., McGinnis, S., Gomperts, S.N., Sepulcre, J., Gomez-Isla, T., Hyman, B.T., Schultz, A., Vasdev, N., Johnson, K.A., Dickerson, B.C., 2017. Association of in vivo [18F]AV-1451 tau PET imaging results with cortical atrophy and symptoms in typical and atypical alzheimer disease. JAMA Neurol. 74, 427–436.
Zhukareva, V., Mann, D., Pickering-Brown, S., Uryu, K., Shuck, T., Shah, K., Grossman, M., Miller, B.L., Hulette, C.M., Feinstein, S.C., Trojanowski, J.Q., Lee, V.M., 2002. Sporadic Pick's disease: a tauopathy characterized by a spectrum of pathological tau isoforms in gray and white matter. Ann. Neurol. 51, 730–739.